Published in final edited form as:
J Comp Neurol. 2010 December 15; 518(24): 4842–4854. doi:10.1002/cne.22491.

Expression Pattern of Membrane-Associated Guanylate Kinases in Interneurons of the Visual Cortex

Gulcan Akgul[1] and **Lonnie P. Wollmuth**[2,*]

[1]Graduate Program in Molecular and Cellular Biology, State University of New York at Stony Brook, Stony Brook, New York 11794-5230

[2]Department of Neurobiology and Behavior, State University of New York at Stony Brook, Stony Brook, New York 11794-5230

Abstract

GABAergic interneurons are key elements regulating the activity of local circuits, and abnormal inhibitory circuits are implicated in certain psychiatric and neurodevelopmental diseases. The glutamatergic input that interneurons receive is a key determinant of their activity, yet its molecular structure and development, which are often distinct from those of glutamatergic input to pyramidal cells, are poorly defined. The membrane-associated guanylate kinase (MAGUK) homologs PSD-95/SAP90, PSD-93/chapsyn110, SAP97, and SAP102 are central organizers of the postsynaptic density at excitatory synapses on pyramidal neurons. We therefore studied the cell-type-specific and developmental expression of MAGUKs in the nonoverlapping parvalbumin (PV)- and somatostatin (SOM)-positive interneurons in the visual cortex. These interneuron subtypes account for the vast majority of interneurons in the cortex and have different functional properties and postsynaptic structures, being either axodendritic (PV^+) or axospinous (SOM^+). To study cell-type-specific MAGUK expression, we used DIG-labeled riboprobes against each MAGUK along with antibodies against either PV or SOM and examined tissue from juvenile (P15) and adult mice. Both PV^+ and SOM^+ interneurons express mRNA for PSD-95, PSD-93, and SAP102 in P15 and adult tissue. In contrast, these interneuron subtypes express SAP97 at P15, but for adult visual cortex we found that most PV^+ and SOM^+ interneurons show low or no expression of SAP97. Given the importance of SAP97 in regulating AMPA receptor GluA1 subunit and NMDA receptor subunits at glutamatergic synapses, these results suggest a developmental shift in glutamate receptor subunit composition and regulation of glutamatergic synapses on PV^+ and SOM^+ interneurons.

Indexing terms

parvalbumin-positive; somatostatin-positive; in situ hybridization; PSD-95; PSD-93; SAP97; SAP102

In the cortex, a variety of biochemically, morphologically, and functionally distinct subtypes of GABAergic interneurons regulate the activity of local microcircuits (Markram et al., 2004; Silberberg et al., 2005). The excitatory glutamatergic input onto cortical interneurons is a key determinant of their function and can be altered with activity (Kullmann and Lamsa, 2007) and development (Hennou et al., 2002). In addition, abnormal inhibitory

*Correspondence To: Dr. Lonnie P. Wollmuth, Department of Neurobiology and Behavior and Center for Nervous System Disorders, State University of New York at Stony Brook, Stony Brook, NY 11794-5230. lwollmuth@notes.cc.sunysb.edu.

Additional Supporting Information may be found in the online version of this article.

(GABAergic) circuits are implicated in certain psychiatric and neurodevelopmental diseases, such as schizophrenia and autism (Di Cristo, 2007; Lisman et al., 2008). Schizophrenia, for example, may reflect in part a decreased glutamatergic innervation and NMDAR expression on GABAergic interneurons in the prefrontal cortex (Lisman et al., 2008). Still, despite their important role in regulating GABAergic activity, the molecular structure, development, and dynamics of glutamatergic synapses on inter-neurons are poorly defined. Although glutamatergic synapses on interneurons may share key features and mechanisms with pyramidal neurons, GABAergic inter-neuron subtypes often express distinct glutamate receptor subunits (e.g., only Ca^{2+}-permeable AMPAR subunits and the NMDAR GluN2C subunit; Geiger et al., 1995; Angulo et al., 1997; Moga et al., 2002; Martina et al., 2003), can lack spines (Kawaguchi and Kubota, 1993; Goldberg et al., 2003; Goldberg and Yuste, 2005), and can show distinct features of synaptic plasticity (Kullmann and Lamsa, 2007; Nissen et al., 2010).

Membrane-associated guanylate kinases (MAGUKs) are scaffolding proteins and central organizers of glutamatergic synapses. The MAGUK family has four members that can be expressed in the postsynaptic density (PSD) of excitatory synapses: PSD-95, PSD-93, SAP97, and SAP102 (Funke et al., 2005; Sheng and Hoogenraad, 2007). These proteins share high sequence similarity as well as similar domain structure: three PDZ domains followed by an SH3 and a GK domain (Funke et al., 2005; Sheng and Hoogenraad, 2007). In general, these PSD proteins have been implicated in trafficking, clustering, and regulating GluRs (Elias and Nicoll, 2007; Newpher and Ehlers, 2008; Robertson et al., 2009), as intracellular adaptor proteins (Funke et al., 2005), and as elements in brain dysfunction (Gardoni, 2008). They interact with different GluR subunits (Leonard et al., 1998; Kim and Sheng, 2004), GluR-interacting proteins (see, e.g., Chen et al., 2000; Bats et al., 2007), and cytoplasmic proteins (Sheng and Hoogenraad, 2007). Accordingly, they have different functions at specific synapses (Regalado et al., 2006; Elias et al., 2008). In addition, EM studies suggest preferential localization of MAGUK members in different excitatory synapses and subsynaptic compartments (synaptic vs. extrasynaptic; Aoki et al., 2001).

All members of the MAGUK family are expressed in the mouse and rat brain, including the cortex (Kim et al., 1996; Allen Brain Atlas; http://mouse.brain-map.org/). However, they show strong developmental and brain-region- and cell-type-specific expression patterns (Fukaya et al., 1999; Fukaya and Watanabe, 2000; Aoki et al., 2001). In addition, although their cell-type-specific expression can be defined in certain brain regions with well-defined structure (e.g., cerebellum; http://mouse.brain-map.org/; Muller et al., 1995; Brenman et al., 1996; Chetkovich et al., 2002), this is not possible in the cortex, where pyramidal neurons and a variety of interneuron subtypes are mixed together. In the cortex, the two most prominent interneuron subtypes are parvalbumin (PV)- and somatostatin (SOM)-positive. These nonoverlapping interneuron subtypes of the cortex differ not only in terms of biochemical markers but also in morphology, membrane properties, synaptic targeting, and subcellular architecture (Markram et al., 2004; Burkhalter, 2008). PV^+ interneurons are mainly multipolar basket cells that are fast-spiking and that target exclusively perisomatic domains of pyramidal neurons, having a strong influence on action potential generation (Freund, 2003; Freund and Katona, 2007). On the other hand, SOM^+ interneurons are bitufted Martinotti cells that are regular-spiking and that target mainly more distal dendrites, influencing primarily synaptic integration (Thomson and Bannister, 2003; Markram et al., 2004). Notably, glutamatergic synapses on PV^+ interneurons are axodendritic (aspiny), whereas on SOM^+ interneurons they are axospinous (spiny; Kawaguchi and Kubota, 1993; Goldberg and Yuste, 2005). In addition, although the identity of GluR subtypes is not well-defined on these cells, they both express Ca^{2+}-permeable AMPARs (Geiger et al., 1995; Moga et al., 2002).

Given the importance of MAGUKs in organizing and regulating pyramidal-to-pyramidal synapses (Montgomery et al., 2004; Sheng and Hoogenraad, 2007), we defined their cell-type-specific expression profiles in PV^+ and SOM^+ interneurons as a function of developmental age. To do so, we used a combination of in situ hybridization and immunohistochemistry to characterize the mRNA expression pattern of MAGUKs in these interneurons in the visual cortex. Surprisingly, we find that the four MAGUKs show a comparable expression pattern in the two interneuron subtypes. However, SAP97 was developmentally regulated, with a subset of both PV^+ and SOM^+ interneurons showing greatly decreased expression in adult. The identity of these interneuron subsets and the functional consequences of SAP97 absence in adults remain unknown.

Materials and methods

Animals

Maintenance of all animal and the surgical procedures used were approved by the institutional animal care and usage committee at Stony Brook University and were in line with the guidelines established by the National Institutes of Health.

Tissue preparation

Fifteen (juvenile)- or fifty-six (adult)-day-old mice were deeply anesthetized with intraperitoneal administration of ketamine (0.12 cc/100 g) and xylazine (0.05 cc/100 g) and then perfused transcardially with 0.1 M phosphate buffer (PB) and fixed with 4% paraformaldehyde. Brains were dissected out and postfixed in the same fixative for 3 hours at room temperature.

A postfixed brain was left in 30% sucrose solution for dehydration at 4°C and was then cut longitudinally into two hemispheres. A hemisphere was then immersed in Shandon M-1 embedding matrix (Thermo Scientific, Rock-ford, IL) and cryosectioned at −20°C (Leica LM1850; Leica Microsystems, Bannockburn, IL) at 20 μm thick. Sections were kept in cryobuffer (27% glycerol, 27% ethylene glycerol) at −20°C. All solutions were DEPC-treated and autoclaved to avoid RNA degradation by RNases.

Antibodies

The following primary antibodies were used: rabbit polyclonal anti-PV (Abcam, Cambridge, MA) and rat monoclonal anti-SOM (Chemicon, Temecula, CA; Table 1). As secondaries, we used fluorescent Alexa 488-conjugated anti-rabbit and anti-rat IgG (Molecular Probes, Eugene, OR) or alkaline phosphatase-conjugated anti-DIG (anti-DIG-AP; Roche Applied Science, Indianapolis, IN) and hydrogen peroxide-conjugated anti-DIG (anti-DIG-POD; Roche Applied Science).

Table 1 summarizes the source, properties, and dilution of the antibodies used in the present study. Rabbit anti-PV recognizes a single band on a Western blot of rat cerebellar tissue extract and also labels a subset of GABAergic interneurons in mouse cortical tissue (manufacturer's data sheet). Immunolabeling is consistent with previous studies (Supp. Info. Figs. 3, 5). Rat anti-SOM recognizes a single ~17-kDa band of the molecular weight marker on the Western blot of mouse brain tissue extract. Although the published data on the brain tissue proposes a dominant 15-kDa band for somatostatin (Morel et al., 1983), higher molecular weight bands were observed in human and fish tissue (Shields, 1980; Levy et al., 1993). Immunolabeling is consistent with previous results (Supp. Info. Figs. 4, 5).

In situ hybridization

Probes—Antisense riboprobes for each gene were transcribed with T7 RNA polymerase (Roche Applied Science) in the presence of digoxigenin-11-UTP (Roche Applied Science). Digoxigenin-labeled RNA probes were purified with Centri-Sep spin columns (Princeton Separations, Adelphia, NJ). Resulting probes were tested for RNA integrity and size by electrophoresis (1% agarose gel). For quantification, serial dilutions of the probes as well as the DIG-labeled control RNA were UV-linked onto the nylon membranes. Alkaline phophatase-conjugated anti-DIG fragments (Roche Applied Science) were used to detect digoxigenin incorporated into the probes. Digoxigeninantibody complexes were further incubated with NBT/BCIP substrate, and color change was monitored. Estimations of probe concentrations were made based on the control RNA signals on the membrane.

Riboprobes for each MAGUK (PSD-95, PSD-93, SAP97, and SAP102) were designed based on the analysis of their cDNA sequence alignments. Both α and β isoforms of PSD-95 and SAP97 (Chetkovich et al., 2002; Schluter et al., 2006; Waites et al., 2009) are targeted with their respective riboprobes. The following PCR primers were used for the probe synthesis: PSD-95 forward: ATGCTCCCCCAGACATCACAA; PSD-95 reverse: CCAAGG ATGATGATGGGACGA; PSD-93 forward: GCTGCACAGAAA GATGGGAGG; PSD-93 reverse: GGAGCCTTTGTGAAGGAC CAC; SAP97 forward: TCGGGTCTTGGTTTCAGC; SAP97 reverse: GGCGGACCTGCTGATCTA; SAP102 forward: GAC GTCCATCAACGGTAC; SAP102 reverse: CAGCTTGTACT CTCTGCC.

Specificity controls—Specificity of the riboprobes was further tested with dot blot analysis. Serial dilutions (0.001-10 ng) of full-length mRNA of each MAGUK were UV-linked to a nylon membrane and hybridized with DIG-labeled riboprobes under the same conditions as in the in situ hybridization on the tissues. Each antisense riboprobe hybridized, in a concentration-dependent manner (based on increasing intensity), with its complementary MAGUK transcript. Hybridizations with nontarget MAGUKs either were not detected or occurred only at high concentrations of the transcript (10 ng; Supp. Info. Fig. 1). In addition, our riboprobes recapitulate layer- and cell-type-specific expression in the cerebellum (Supp. Info. Fig. 2).

Hybridization—Before hybridization, tissue sections were washed with phosphate-buffered saline (PBS), placed on precleaned slides, and air dried. Sections were then digested with predigested proteinase-K (20 μg/ml) for 7 minutes and then postfixed with cold 4% paraformaldehyde for 10 minutes at room temperature. Postfixed tissue sections were acetylated for 10 minutes and washed in 1× Tris/glycine (pH 7.0) for 30 minutes at room temperature. Washes between each application were performed with 1 × PBS. Sections were then prehybridized for 2 hours at 65°C in a hybridization solution (50% formamide, 4× SSC, 5× Denhardt's solution, yeast RNA, salmon sperm DNA, dextran sulfate) without probe and hybridized with 500 ng DIG-labeled probe in the same hybridization solution overnight at 65°C in a humidified chamber. Sense probes, a probe targeting *Xenopus laevis* heterogeneous nuclear ribonucleoprotein A/B (hnrpab) gene, and a hybridization reaction without any probe were used as controls. Posthybridization treatments included washes in 50% formamide/2× SSC at 65°C and RNaseA digestion (Sigma-Aldrich, St. Louis, MO) at 37°C.

Successful hybridizations were detected with anti-DIG fragments. Tissue was blocked for 30 minutes in blocking solution (100 mM Tris-Cl, pH 7.5, 150 mM NaCl, 0.5% Triton X-100, 2% normal sheep serum). Tissue sections were then incubated with a polyclonal antibody against digoxigenin conjugated to either alkaline phosphatase (1:1,000) or hydrogen peroxide (1:100).

For chromogenic detection, sections were incubated in color-detection buffer (100 mM Tris-Cl, pH 9.5, 100 mM NaCl) containing NBT/BCIP. After color development, sections were left to dry overnight and mounted with Permount (Fisher Scientific, Pittsburgh, PA). For fluorescent detection, sections were incubated with fluorescent detection buffer (100 mM Tris-Cl, pH 8.0, 100 mM NaCl, 10 mM $MgCl_2$) containing either an alkaline phosphatase substrate, HNPP/Fast Red TR Mix (Roche Applied Science), or a hydrogen peroxide substrate, CY3-tyramide signal amplification (TSA-CY3; PerkinElmer, Wellesley, MA). The sections were then mounted with Vectashield mounting medium (Vector Laboratories, Burlingame, CA). Images were taken and analyzed with a Zeiss LSM 510 confocal microscope.

Combined in situ hybridization and immunohistochemistry—In the experiments in which we used both in situ hybridization and immunohistochemistry, the second technique was integrated into the in situ hybridization protocol at the secondary antibody (anti-DIG fragments) incubation step. Anti-PV and anti-SOM antibodies were included in the antibody mix for overnight incubation. After the washes, in situ hybridization signal was developed with either HNPP/Fast Red TR kit or TSA-indirect amplification kit, and the tissues were incubated with fluorescent secondary antibodies to develop immunohistochemistry signal. The sections were then mounted and imaged as noted previously.

Quantification of cell-type-specific expression

Identification of PV^+ and SOM^+ cells was done by means of design-based (assumption-free, unbiased) stereology (Peterson, 1999). Mouse brains from at least three different animals were used for each condition. Sections were collected using systematic-random sampling. The 20-μm slices were collected in six parallel sets, each set consisting of 10-14 sections, with each section separated by 120 μm. Among the six sets, four were randomly assigned to a particular MAGUK, and the remaining two sets were used for control experiments or discarded. Analysis of signal intensities for in situ hybridization and immunohistochemistry was done with the Profile Analysis component of LSM 510 software. For each section, only the central focal plane, avoiding the edges of the section, was used for sampling. Stage movements were made by hand to move between nonoverlapping sample fields. For each section, the background intensity was determined on a region where there were no obvious neuronal soma. Each PV^+ and SOM^+ interneuron (intensity at least 50% greater than background) with a well-defined nucleus was scored for MAGUK expression. Lines were drawn through the cell using at least three different angles (see Fig. 3). When peaks for the MAGUK signal for at least one of these lines were 50% more than the background and paralleled the PV^+ and SOM^+ distribution, they were scored positive. In certain instances, it was impossible to score a cell as MAGUK-positive or -negative because of adjacent cells or the overall positioning of the PV^+ or SOM^+ soma. These cases were recorded as ambiguous.

Results

By using a combination of in situ hybridization and immunohistochemistry, we characterized the cell-type-specific mRNA expression of four MAGUKs (PSD-95, PSD-93, SAP97, SAP102) in PV^+ and SOM^+ interneurons in mouse brain, focusing on the visual cortex. We selected layers 2/3 and layer 5 to be representative of the cortex and monitored age dependence by measuring expression in both juvenile (P15) and adult mouse brains. We chose P15 as the earliest developmental point because synaptogenesis begins around this time (Miller, 1986), and PV gene expression is turned on in the cortex after P14 (see, e.g., Gonchar et al., 2007).

PV+ and SOM+ interneurons in the visual cortex of juvenile (P15) and adult mice express PSD-95 mRNA

Figures 1 and 2 show confocal images of tissue sections, encompassing the visual cortex, from juvenile (P15; Fig. 1) and adult (Fig. 2) mouse brains labeled with either PV (Figs. 1A1–C3, 2A1–B3) or SOM (Figs. 1D1–F3, 2C1–D3) antibody (green) and hybridized with DIG-labeled PSD-95 riboprobes (red). Figure 1A1–A3,D1–D3 shows images of the visual cortex of a mouse brain at low magnification (×10), with the approximate boundaries of the layers demarcated in Figure 1A3,D3. PV^+ interneurons, which represent about ~40% of cortical $GABA^+$ interneurons, and SOM^+ interneurons (~30%) are dispersed throughout the entire visual cortex (Fig. 1A1,D1; Markram et al., 2004; Gonchar et al., 2007).

Magnified images of cells in layers 2/3 and layer 5 for P15 mouse tissue are shown in Figure 1B1–B3,E1–E3 and Figure 1C1–C3,F1–F3, respectively. Consistent with previous reports (Gonchar et al., 2007), PV staining is observed both in the cytoplasm and in the nucleus (Fig. 1B1,C1). In contrast to PV, SOM staining is restricted to the cytoplasm (Fig. 1E1,F1), as is the signal for PSD-95 (Fig. 1B2,C2,E2,F2). Figure 1B3,C3 shows merged images of the PV and PSD-95 signals with our approach to define overlap between them (shown in Fig. 3). Figure 3A3 shows a merged image (same as Fig. 1B3) of the analyzed cell (for additional details see Materials and Methods). As shown in Figure 3B1-B3, the peak PV signal (green) was used to define the borders of the PV^+ cell (dashed lines), and then the peak MAGUK signal was used, taking into account surrounding cells, to define whether the cell was positive or negative for the MAGUK. In this instance, the PSD-95 signal (red) is clearly located within the PV^+ borders. Among the 32 cells in layers 2/3 and the 28 cells in layer 5 that were positive for PV, almost all scored positive for PSD-95 mRNA in P15 mouse visual cortex (Table 2). In adult mice, a similar expression pattern of PSD-95 was also observed in PV^+ interneurons (Fig. 2A1–B3, Table 2).

Similarly, as shown in the merged images (Fig. 1E3,F3), PSD-95 mRNA colocalizes with the SOM signal, a point further illustrated in the colocalization analysis (Fig. 3C1–D3). Indeed, almost all identified SOM^+ interneurons in layers 2/3 (74 total) and layer 5 (114 total) in P15 mice scored positive for PSD-95 (Table 2). SOM^+ interneurons in adult animals also express PSD-95 mRNA (Fig. 2C1,D3, Table 2). In summary, the nonoverlapping PV^+ and SOM^+ interneuron populations in the cortex both express PSD-95 mRNA at minimum from P15 to adult.

PV+ and SOM+ interneurons in the visual cortex of juvenile (P15) and adult mice express PSD-93 mRNA

Figure 4 shows cell-type-specific PSD-93 mRNA expression for PV^+ (Fig. 4A1–B3) and SOM^+ (Fig. 4C1–D3) interneurons in layers 2/3 of P15 (Fig. 4A1-A3,C1-C3) and adult (Fig. 4B1–B3,D1–D3) mouse visual cortex. PSD-93 shows wide cellular expression in both P15 (Fig. 4A2,C2) and adult (Fig. 4B2,D2) tissue. The merged images show that PSD-93 mRNA colocalizes with PV in P15 (Fig. 4A3) and adult (Fig. 4B3) tissue (colocalization analysis not shown). Over 90% of PV^+ cells in both P15 and adult tissue scored positive for PSD-93 mRNA (Table 2). PV^+ interneurons in layer 5 showed a similar strong colocalization (data not shown; Table 2). For P15 and adult SOM^+ interneurons, PSD-93 mRNA is also expressed in layers 2/3 (Fig. 4C1–D3) and layer 5 (data not shown; Table 2). Therefore, like PSD-95, both PV^+ and SOM^+ interneurons express PSD-93 mRNA at P15 and adult.

PV+ and SOM+ interneurons in the visual cortex of juvenile (P15) and adult mice express SAP102 mRNA

Figure 5 shows cell-type-specific SAP102 mRNA expression for PV^+ (Fig. 5A1–B3) and SOM^+ (Fig. 5C1–D3) interneurons in layers 2/3 of P15 (Fig. 5A1–A3,C1–C3) and adult

(Fig. 5B1–B3,D1–D3) mouse visual cortex. In contrast to other MAGUKs, SAP102 in situ hybridization gave punctate staining probably because of the different signal detection technique used (TSA-CY3; see Material and Methods), which provides increased sensitivity (Breininger and Baskin, 2000). Nevertheless, as shown in the merged images, these punctate signals showed a clear overlap with PV in P15 (Fig. 5A3) and adult (Fig. 5B3) tissue (colocalization analysis not shown). Over 85% of PV^+ cells in both P15 and adult tissue scored positive for SAP102 mRNA (Table 2). PV^+ interneurons in layer 5 showed a similar strong colocalization (data not shown; Table 2). For P15 and adult, SAP102 mRNA is also colocalized with SOM in layers 2/3 (Fig. 5C1-D3) and layer 5 (data not shown; Table 2). Therefore, both PV^+ and SOM^+ interneurons express SAP102 mRNA at P15 and adult.

SAP97 mRNA shows a developmental expression pattern in both PV^+ and SOM^+ interneurons in the visual cortex

Figure 6 shows cell-type-specific SAP97 mRNA expression for PV^+ (Fig. 6A1–B3) and SOM^+ (Fig. 6C1–E3) interneurons in layers 2/3 of P15 (Fig. 6A1-A3,C1-C3) and adult (Fig. 6B1-B3,D1-E3) visual cortex. In P15 tissue, the merged images show that SAP97 mRNA colocalizes with PV and SOM (Fig. 6A3,C3), a result also found in layer 5 (Supp. Info. Fig. 6C,F). Indeed, over 85% of cells positive for PV or SOM in layers 2/3 and layer 5 in P15 tissue scored positive for SAP97 mRNA (Table 2).

In adult tissue, on the other hand, most PV^+ and SOM^+ interneurons scored negative for SAP97. For PV (Fig. 6B1– B3), the triangles point to a representative PV^+ cell that was scored negative for SAP97, whereas the arrowhead indicates a PV^+ cell that scored positive. This point is illustrated more specifically in Figure 7, which shows the quantitative analysis for the PV^+ cells that are either negative [Fig. 7A1–A3,B; note the ab sence of a higher intensity halo/ring around the nucleus especially in regions remote from the two adjacent cells and that no SAP97 signal (red) was above baseline in association with the PV signal as illustrated in Fig. 7B] or positive (Fig. 7C1–C3,D; note the halo/ring around the nucleus that is greater than the background and is associated with the PV signal as illustrated in Fig. 7D) for SAP97.

Expression of SAP97 in SOM^+ cells in adult tissue (Fig. 6D1–D3) was also restricted. Figure 6D1–D3 indicates a SOM^+ cell that is negative for SAP97 hybridization (triangle; for quantification analysis see Fig. 7E1-E3,F), and Figure 6E1-E3 indicates a SOM^+ cell that is positive for SAP97 hybridization (arrowhead; see Fig. 7G1-G3,H). In adult tissue, over 60% of PV^+ or SOM^+ interneurons in layers 2/3 and layer 5 scored negative for SAP97 mRNA (Table 2).

The developmental regulation of SAP97 mRNA expression in mouse visual cortex also occurs in layer 5, with Figure 8 illustrating examples of PV^+ and SOM^+ interneurons with low and high SAP97 expression levels. Figure 8A1,A3 shows PV^+ cells scored negative (triangle) and positive (arrow) for SAP97. The colocalization analysis of PV and SAP97 signals is represented in Figure 8D1-D3,E,F1-F3,G (note the absence of halo/ring for SAP97 signal around the nucleus of the neuron in Fig. 8D1-D3). Figure 8B1–B3 shows an example of SOM^+ interneurons in layer 5 that scored negative for SAP97 and Figure 8C1-C3 shows SOM^+ interneurons that scored positive for SAP97.

Discussion

By using combined in situ hybridization and immunohistochemistry, we demonstrate for the first time the cell-type-specific expression of MAGUKs in cortical interneurons, specifically, those positive for PV or SOM. Surprisingly, although the glutamatergic synapses on PV^+ and SOM^+ interneurons show distinct morphological and functional

properties (see the introductory paragraphs), they express all four MAGUKs comparably, with a subset of both subtypes showing a reduced expression of SAP97 in adult animal. Although the four MAGUKs are structurally similar, our riboprobes were highly specific (see Materials and Methods) and did not show any obvious cross-reactivity (Supp. Info. Fig. 1). In addition, the MAGUKs do show cell-type-specific expression in the brain (see the introductory paragraphs), and our riboprobes confirm these ideas in the cerebellum (Supp. Info. Fig. 2; Muller et al., 1995; Brenman et al., 1996; Chetkovich et al., 2002). Thus, the expression patterns of the various MAGUKs in PV^+ and SOM^+ interneurons are specific, although their functional significance, their specific subcellular distributions, and the developmental role of changes in SAP97 expression remain unknown. Finally, although our experiments were done on the visual cortex, our results are applicable more widely to all PV^+ and SOM^+ interneurons in the cerebral cortex.

Interneuron subtypes in the visual cortex

In the mouse visual cortex, various subtypes of GABAergic interneurons have been characterized on the basis of the combinations of biochemical markers that they express, such as PV, SOM, calretinin (CR), neuropeptide-Y (NPY), vasoactive intestinal polypeptide (VIP), and cholecystokinin (CCK), among others (Markram et al., 2004; Burkhalter, 2008). These subtypes often show different physiological and anatomical properties. We studied PV^+ (fast-spiking) and SOM^+ (regular-spiking) interneurons because they constitute a majority (~65%) of the interneurons in the cortex (Gonchar et al., 2007). In addition, they present an interesting structural contrast in their glutamatergic synapses: PV^+ interneurons are aspiny, whereas SOM^+ interneurons form spiny synapses (Kawaguchi and Kubota, 1993; Goldberg and Yuste, 2005). In our study, we screened MAGUK mRNA expression at P15, the age when eye-opening occurs with initiation of activity-dependent plasticity, and PV^+ and SOM^+ interneurons are still relatively immature, as well as in adult tissue.

MAGUK expression in PV^+ and SOM^+ interneurons

We used riboprobes to detect MAGUK mRNA in mouse brain tissue. The advantage of in situ hybridization is that mRNA is found mostly in the cell soma and is easy to colocalize with cellular markers (i.e., PV and SOM). However, although in situ hybridization indicates gene expression, it does not indicate protein expression or the distribution of proteins at a synapse.

Our experiments show that both PV^+ and SOM^+ interneurons express PSD-95 (Figs 1–3, Table 2), PSD-93 (Fig. 4, Table 2), and SAP102 (Fig. 5, Table 2) mRNA at all ages tested (P15 and adult). Indeed, in almost all instances, the MAGUK signal colocalized with the interneuron marker >90% of the time. SAP97, on the other hand, is strongly expressed in both interneuron subtypes at P15 (Figs. 6, 7, Table 2, Supp. Info. Fig. 6), but its expression drops to an undetectable level in more than half (approximately 60%) of the interneurons in adult animals (Figs. 6, 7, Table 2, Supp. Info. Fig. 6). Either the interneurons do not express the mRNA at all or its expression is too low to be detected with the tools that we used.

Interneuron groups that are defined with certain biochemical markers can often be divided into further subtypes based on coexpression with another biochemical marker (Markram et al., 2004; Gonchar et al., 2007; Burkhalter, 2008). For example, SOM^+ interneurons partially overlap with CR^+ interneurons (Gonchar et al., 2007). SAP97 expression in adult animals may be restricted to such a subgroup of PV^+ and SOM^+ interneurons. However, because PV^+ and SOM^+ interneurons do not overlap (Gonchar et al., 2007; Supp. Info. Fig. 5) and no known biochemical marker is common to both subtypes, it is presently not clear what this additional marker might be. Nevertheless, given the key role of SAP97 in regulating AMPA and NMDA receptors at glutamatergic synapses (see below), it will be

critical to define the functional significance of these distinct classes of PV^+ and SOM^+ interneurons in adult.

Functional significance of MAGUKs at glutamatergic synapses on interneurons

A major group of interacting partners of MAGUKs are GluRs. MAGUKs bind directly to NMDA receptor subunits (Kim and Sheng, 2004; Gardoni, 2008) and associate with AMPA receptors typically via TARPs (Chen et al., 2000). The exception of course is SAP97, the only MAGUK that can bind directly to AMPA receptors, specifically, GluA1 (Leonard et al., 1998; Sans et al., 2001). Overexpression of SAP97 increases the number of GluA1-containing AMPA receptors at synaptic sites on pyramidal neurons as a result of enhanced trafficking and clustering of the receptors (Rumbaugh et al., 2003; Waites et al., 2009). Additionally, SAP97 is involved in the sorting and trafficking of NMDA receptors to glutamatergic synapses on pyramidal neurons (Jeyifous et al., 2009). The expression of GluR subtypes and subunits at glutamatergic synapses on interneurons is often different from that on pyramidal neurons (see, e.g., Geiger et al., 1995; Moga et al., 2002; Martina et al., 2003). For example, NMDA receptor expression in PV^+ and SOM^+ interneurons of rat hippocampus is lower than in pyramidal neurons (Nyiri et al., 2003), and the GluN2C index is higher (Martina et al., 2003). In addition, they often express Ca^{2+}-permeable AMPA receptor subunit combinations (GluA1, -A3, and/or -A4; Geiger et al., 1995; Angulo et al., 1997; Moga et al., 2002). Nevertheless, subunit-specific expression patterns of GluRs in interneurons are not well defined. The subunit-specific expression of the receptors might be correlating with the expression of MAGUKs in the interneurons and could possibly be related to changes in interneuron excitation during the critical period of visual cortex plasticity (Maffei and Turrigiano, 2008) Nevertheless, additional experiments will be needed to define this relationship.

Dysfunction of GABAergic interneurons is implicated in neurodevelopmental and psychiatric disorders (Di Cristo, 2007; Lisman et al., 2008). In addition, decreased NMDAR expression level is prominent in psychiatric diseases such as schizophrenia and bipolar disorder (Kristiansen et al., 2007; Lisman et al., 2008). In parallel, abnormal MAGUK expression levels are observed in various brain regions in these psychiatric diseases (see, e.g., Kristiansen et al., 2007). Low expression and activity of NMDARs and GABAergic interneurons might be the result of dysfunction of MAGUKs at the glutamatergic synapses onto these interneurons. Understanding glutamate receptor trafficking and synaptic activity in GABAergic interneurons will be essential to comprehending the regulation of interneuron activity and the role in disease development.

In conclusion, our study demonstrates the interneuronal expression pattern of MAGUKs at the mRNA level in mouse visual cortex of juvenile (P15) and adult animals. Although we showed a broad mRNA expression of MAGUKs in PV^+ and SOM^+ interneurons, the synaptic localization of their protein expression, the interaction of MAGUKs with specific GluRs at interneuron synapses, and the potential contribution of MAGUKs to the structure and function of aspiny and spiny glutamatergic synapses on interneurons remain unknown.

Supplementary Material

Refer to Web version on PubMed Central for supplementary material.

Acknowledgments

We thank Aiying Liu and Dr. Mary Kritzer for technical assistance with immunohistochemistry; Janet Allopenna and Dr. Kyungmin Ji for technical assistance with in situ hybridization; Dr. Juan M. Encinas for assistance with cell quantification; and Dr. Mark Bowen, Catherine L. Salussolia, and Jessica Helm for their comments on the manuscript.

Grant sponsor: National Eye Institute; Grant number: EYO1697905 (to L.P.W.).

Literature cited

Angulo MC, Lambolez B, Audinat E, Hestrin S, Rossier J. Subunit composition, kinetic, and permeation properties of AMPA receptors in single neocortical nonpyramidal cells. J Neurosci. 1997; 17:6685–6696. [PubMed: 9254681]

Aoki C, Miko I, Oviedo H, Mikeladze-Dvali T, Alexandre L, Sweeney N, Bredt DS. Electron microscopic immunocytochemical detection of PSD-95, PSD-93, SAP-102, and SAP-97 at postsynaptic, presynaptic, and nonsynaptic sites of adult and neonatal rat visual cortex. Synapse. 2001; 40:239–257. [PubMed: 11309840]

Bats C, Groc L, Choquet D. The interaction between stargazin and PSD-95 regulates AMPA receptor surface trafficking. Neuron. 2007; 53:8.

Breininger JF, Baskin DG. Fluorescence in situ hybridization of scarce leptin receptor mRNA using the enzyme-labeled fluorescent substrate method and tyramide signal amplification. J Histochem Cytochem. 2000; 48:1593–1599. [PubMed: 11101627]

Brenman JE, Christopherson KS, Craven SE, McGee AW, Bredt DS. Cloning and characterization of postsynaptic density 93, a nitric oxide synthase interacting protein. J Neurosci. 1996; 16:7407–7415. [PubMed: 8922396]

Burkhalter A. Many specialists for suppressing cortical excitation. Front Neurosci. 2008; 2:155–167. [PubMed: 19225588]

Chen L, Chetkovich DM, Petralia RS, Sweeney NT, Kawasaki Y, Wenthold RJ, Bredt DS, Nicoll RA. Stargazin regulates synaptic targeting of AMPA receptors by two distinct mechanisms. Nature. 2000; 408:936–943. [PubMed: 11140673]

Chetkovich DM, Bunn RC, Kuo SH, Kawasaki Y, Kohwi M, Bredt DS. Postsynaptic targeting of alternative postsynaptic density-95 isoforms by distinct mechanisms. J Neurosci. 2002; 22:6415–6425. [PubMed: 12151521]

Di Cristo G. Development of cortical GABAergic circuits and its implications for neurodevelopmental disorders. Clin Genet. 2007; 72:1–8. [PubMed: 17594392]

Elias GM, Nicoll RA. Synaptic trafficking of glutamate receptors by MAGUK scaffolding proteins. Trends Cell Biol. 2007; 17:343–352. [PubMed: 17644382]

Elias GM, Elias LA, Apostolides PF, Kriegstein AR, Nicoll RA. Differential trafficking of AMPA and NMDA receptors by SAP102 and PSD-95 underlies synapse development. Proc Natl Acad Sci U S A. 2008; 105:20953–20958. [PubMed: 19104036]

Freund TF. Interneuron Diversity Series: rhythm and mood in perisomatic inhibition. Trends Neurosci. 2003; 26:489–495. [PubMed: 12948660]

Freund TF, Katona I. Perisomatic inhibition. Neuron. 2007; 56:33–42. [PubMed: 17920013]

Fukaya M, Watanabe M. Improved immunohistochemical detection of postsynaptically located PSD-95/SAP90 protein family by protease section pretreatment: a study in the adult mouse brain. J Comp Neurol. 2000; 426:572–586. [PubMed: 11027400]

Fukaya M, Ueda H, Yamauchi K, Inoue Y, Watanabe M. Distinct spatiotemporal expression of mRNAs for the PSD-95/SAP90 protein family in the mouse brain. Neurosci Res. 1999; 33:111–118. [PubMed: 10211776]

Funke L, Dakoji S, Bredt DS. Membrane-associated guanylate kinases regulate adhesion and plasticity at cell junctions. Annu Rev Biochem. 2005; 74:219–245. [PubMed: 15952887]

Gardoni F. MAGUK proteins: new targets for pharmacological intervention in the glutamatergic synapse. Eur J Pharmacol. 2008; 585:147–152. [PubMed: 18367167]

Geiger JRP, Melcher T, Koh DS, Sakmann B, Seeburg PH, Jonas P, Monyer H. Relative abundance of subunit mRNAs determines gating and Ca^{2+} permeability of AMPA receptors in principal neurons and interneurons in rat CNS. Neuron. 1995; 15:193–204. [PubMed: 7619522]

Goldberg JH, Yuste R. Space matters: local and global dendritic Ca^{2+} compartmentalization in cortical interneurons. Trends Neurosci. 2005; 28:158–167. [PubMed: 15749170]

Goldberg JH, Tamas G, Aronov D, Yuste R. Calcium microdomains in aspiny dendrites. Neuron. 2003; 40:807–821. [PubMed: 14622584]

Gonchar Y, Wang Q, Burkhalter A. Multiple distinct subtypes of GABAergic neurons in mouse visual cortex identified by triple immunostaining. Front Neuroanat. 2007; 1:3. [PubMed: 18958197]

Hennou S, Khalilov I, Diabira D, Ben-Ari Y, Gozlan H. Early sequential formation of functional $GABA_A$ and glutamatergic synapses on CA1 interneurons of the rat foetal hippocampus. Eur J Neurosci. 2002; 16:197–208. [PubMed: 12169102]

Jeyifous O, Waites CL, Specht CG, Fujisawa S, Schubert M, Lin EI, Marshall J, Aoki C, de Silva T, Montgomery JM, Garner CC, Green WN. SAP97 and CASK mediate sorting of NMDA receptors through a previously unknown secretory pathway. Nat Neurosci. 2009; 12:1011–1019. [PubMed: 19620977]

Kawaguchi Y, Kubota Y. Correlation of physiological subgroupings of nonpyramidal cells with parvalbumin- and calbindinD28k-immunoreactive neurons in layer V of rat frontal cortex. J Neurophysiol. 1993; 70:387–396. [PubMed: 8395585]

Kim E, Sheng M. PDZ domain proteins of synapses. Nat Rev Neurosci. 2004; 5:771–781. [PubMed: 15378037]

Kim E, Cho KO, Rothschild A, Sheng M. Heteromultimerization and NMDA receptor-clustering activity of chapsyn-110, a member of the PSD-95 family of proteins. Neuron. 1996; 17:103–113. [PubMed: 8755482]

Kristiansen LV, Huerta I, Beneyto M, Meador-Woodruff JH. NMDA receptors and schizophrenia. Curr Opin Pharmacol. 2007; 7:48–55. [PubMed: 17097347]

Kullmann DM, Lamsa KP. Long-term synaptic plasticity in hippocampal interneurons. Nat Rev Neurosci. 2007; 8:687–699. [PubMed: 17704811]

Leonard AS, Davare MA, Horne MC, Garner CC, Hell JW. SAP97 is associated with the alpha-amino-3-hydroxy-5-methylisoxazole-4-propionic acid receptor GluR1 subunit. J Biol Chem. 1998; 273:19518–19524. [PubMed: 9677374]

Levy L, Bourdais J, Mouhieddine B, Benlot C, Villares S, Cohen P, Peillon F, Joubert D. Presence and characterization of the somatostatin precursor in normal human pituitaries and in growth hormone secreting adenomas. J Clin Endocrinol Metab. 1993; 76:85–90. [PubMed: 8093621]

Lisman JE, Coyle JT, Green RW, Javitt DC, Benes FM, Heckers S, Grace AA. Circuit-based framework for understanding neurotransmitter and risk gene interactions in schizophrenia. Trends Neurosci. 2008; 31:234–242. [PubMed: 18395805]

Maffei A, Turrigiano G. The age of plasticity: developmental regulation of synaptic plasticity in neocortical microcircuits. Prog Brain Res. 2008; 169:211–223. [PubMed: 18394476]

Markram H, Toledo-Rodriguez M, Wang Y, Gupta A, Silberberg G, Wu C. Interneurons of the neocortical inhibitory system. Nat Rev Neurosci. 2004; 5:793–807. [PubMed: 15378039]

Martina M, Krasteniakov NV, Bergeron R. D-serine differently modulates NMDA receptor function in rat CA1 hippocampal pyramidal cells and interneurons. J Physiol. 2003; 548:411–423. [PubMed: 12611916]

Miller MW. Maturation of rat visual cortex. III. Postnatal morphogenesis and synaptogenesis of local circuit neurons. Brain Res. 1986; 390:271–285. [PubMed: 2420416]

Moga D, Hof PR, Vissavajjhala P, Moran TM, Morrison JH. Parvalbumin-containing interneurons in rat hippocampus have an AMPA receptor profile suggestive of vulnerability to excitotoxicity. J Chem Neuroanat. 2002; 23:249–253. [PubMed: 12048108]

Montgomery JM, Zamorano PL, Garner CC. MAGUKs in synapse assembly and function: an emerging view. Cell Mol Life Sci. 2004; 61

Morel A, Nicolas P, Cohen P. Evidence for a predominant form of Mr = 15,000 prosomatostatin in the mouse hypothalamus. Relationship with somatostatin-14 and -28. J Biol Chem. 1983; 258:8273–8276. [PubMed: 6134727]

Muller BM, Kistner U, Veh RW, Cases-Langhoff C, Becker B, Gundelfinger ED, Garner CC. Molecular characterization and spatial distribution of SAP97, a novel presynaptic protein homologous to SAP90 and the Drosophila discs-large tumor suppressor protein. J Neurosci. 1995; 15:2354–2366. [PubMed: 7891172]

Newpher TM, Ehlers MD. Glutamate receptor dynamics in dendritic microdomains. Neuron. 2008; 58:472–497. [PubMed: 18498731]

Nissen W, Szabo A, Somogyi J, Somogyi P, Lamsa KP. Cell type-specific long-term plasticity at glutamatergic synapses onto hippocampal interneurons expressing either parvalbumin or CB1 cannabinoid receptor. J Neurosci. 2010; 30:1337–1347. [PubMed: 20107060]

Nyiri G, Stephenson FA, Freund TF, Somogyi P. Large variability in synaptic N-methyl-D-aspartate receptor density on interneurons and a comparison with pyramidal-cell spines in the rat hippocampus. Neuroscience. 2003; 119:347–363. [PubMed: 12770551]

Peterson DA. Quantitative histology using confocal microscopy: implementation of unbiased stereology procedures. Methods. 1999; 18:493–507. [PubMed: 10491280]

Regalado MP, Terry-Lorenzo RT, Waites CL, Garner CC, Malenka RC. Transsynaptic signaling by postsynaptic synapse-associated protein 97. J Neurosci. 2006; 26:2343–2357. [PubMed: 16495462]

Robertson HR, Gibson ES, Benke TA, Dell'Acqua ML. Regulation of postsynaptic structure and function by an A-kinase anchoring protein-membrane-associated guanylate kinase scaffolding complex. J Neurosci. 2009; 29:7929–7943. [PubMed: 19535604]

Rumbaugh G, Sia GM, Garner CC, Huganir RL. Synapse-associated protein-97 isoform-specific regulation of surface AMPA receptors and synaptic function in cultured neurons. J Neurosci. 2003; 23:4567–4576. [PubMed: 12805297]

Sans N, Racca C, Petralia RS, Wang YX, McCallum J, Went-hold RJ. Synapse-associated protein 97 selectively associates with a subset of AMPA receptors early in their biosynthetic pathway. J Neurosci. 2001; 21:7506–7516. [PubMed: 11567040]

Schluter OM, Xu W, Malenka RC. Alternative N-terminal domains of PSD-95 and SAP97 govern activity-dependent regulation of synaptic AMPA receptor function. Neuron. 2006; 51:99–111. [PubMed: 16815335]

Sheng M, Hoogenraad CC. The postsynaptic architecture of excitatory synapses: a more quantitative view. Annu Rev Biochem. 2007; 76:823–847. [PubMed: 17243894]

Shields D. In vitro biosynthesis of fish islet preprosomatostatin: evidence of processing and segregation of a high molecular weight precursor. Proc Natl Acad Sci U S A. 1980; 77:4074–4078. [PubMed: 6107904]

Silberberg G, Grillner S, LeBeau FE, Maex R, Markram H. Synaptic pathways in neural microcircuits. Trends Neurosci. 2005; 28:541–551. [PubMed: 16122815]

Thomson AM, Bannister AP. Interlaminar connections in the neocortex. Cereb Cortex. 2003; 13:5–14. [PubMed: 12466210]

Waites CL, Specht CG, Hartel K, Leal-Ortiz S, Genoux D, Li D, Drisdel RC, Jeyifous O, Cheyne JE, Green WN, Montgomery JM, Garner CC. Synaptic SAP97 isoforms regulate AMPA receptor dynamics and access to presynaptic glutamate. J Neurosci. 2009; 29:4332–4345. [PubMed: 19357261]

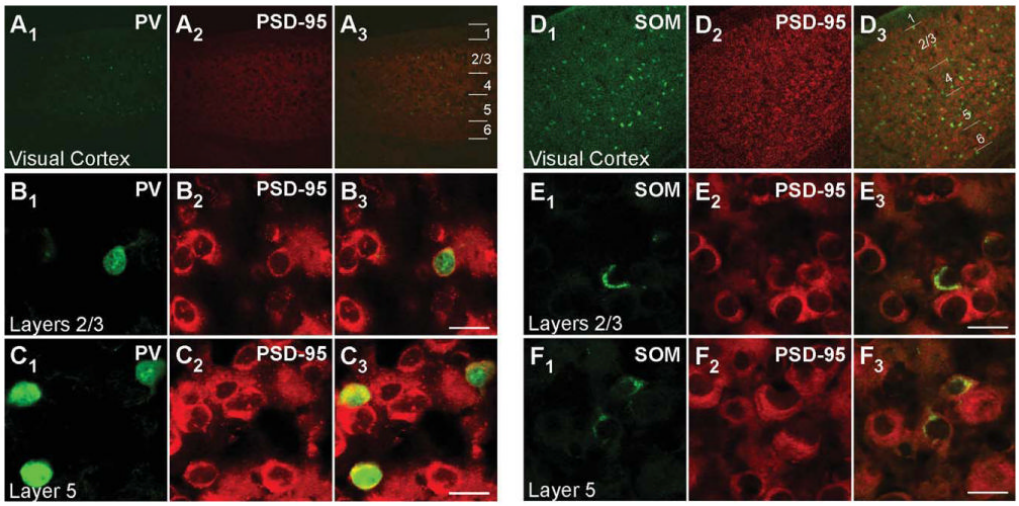

Figure 1.

PSD–95 mRNA expression in PV^+ and SOM^+ interneurons in juvenile (P15) mouse visual cortex. Confocal images of combined in situ hybridization and immunohistochemistry for PSD–95 and either PV or SOM in the mouse visual cortex. Tissue sections were obtained from juvenile (P15) mouse visual cortex. In the left columns, sections were labeled with rabbit anti-PV (green; **A1,B1,C1**) or rat anti-SOM (green; **D1,E1,F1**). In the middle columns (**A2,B2,C2,D2,E2,F2**), the same sections were hybridized with DIG-labeled PSD-95 riboprobe (red). Our riboprobe detected both spliced isoforms (α and β) of PSD-95. The right columns (**A3,B3,C3,D3,E3,F3**) show merged images. The visual cortex is shown at low magnification (×10; A1–A3,D1–D3), with approximate boundaries between layers demarcated in A3,D3. Other images are at ×63, highlighting layers 2/3 (B1–B3,E1–E3) or layer 5 (C1–C3,F1–F3) to show cell-type-specific expression of PSD-95. For magenta-green images see Supporting Information Figure 7. Scale bars = 20 μm.

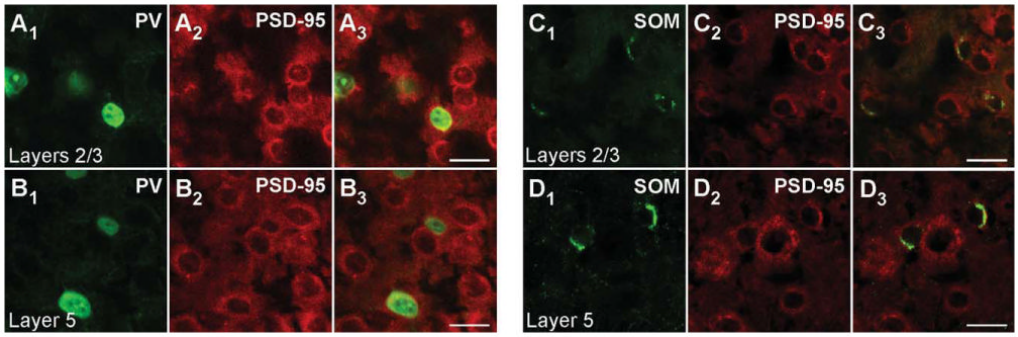

Figure 2.

PSD-95 mRNA in PV^+ and SOM^+ interneurons in adult mouse visual cortex. Confocal images of combined in situ hybridization and immunohistochemistry for PSD-95 and either PV or SOM in the mouse visual cortex. Tissue sections were obtained from adult mouse visual cortex. In the left columns, sections were labeled with rabbit anti-PV (green; **A1,B1**) or rat anti-SOM (green; **C1,D1**). In the middle columns (**A2,B2,C2,D2**), the same sections were hybridized with DIG-labeled PSD-95 riboprobe (red). The right columns (**A3,B3,C3,D3**) show merged images. The images are at ×63, highlighting layers 2/3 (A1-A3,C1-C3) or layer 5 (B1-B3,D1-D3). For magenta-green images see Supporting Information Figure 8. Scale bars = 20 μm.

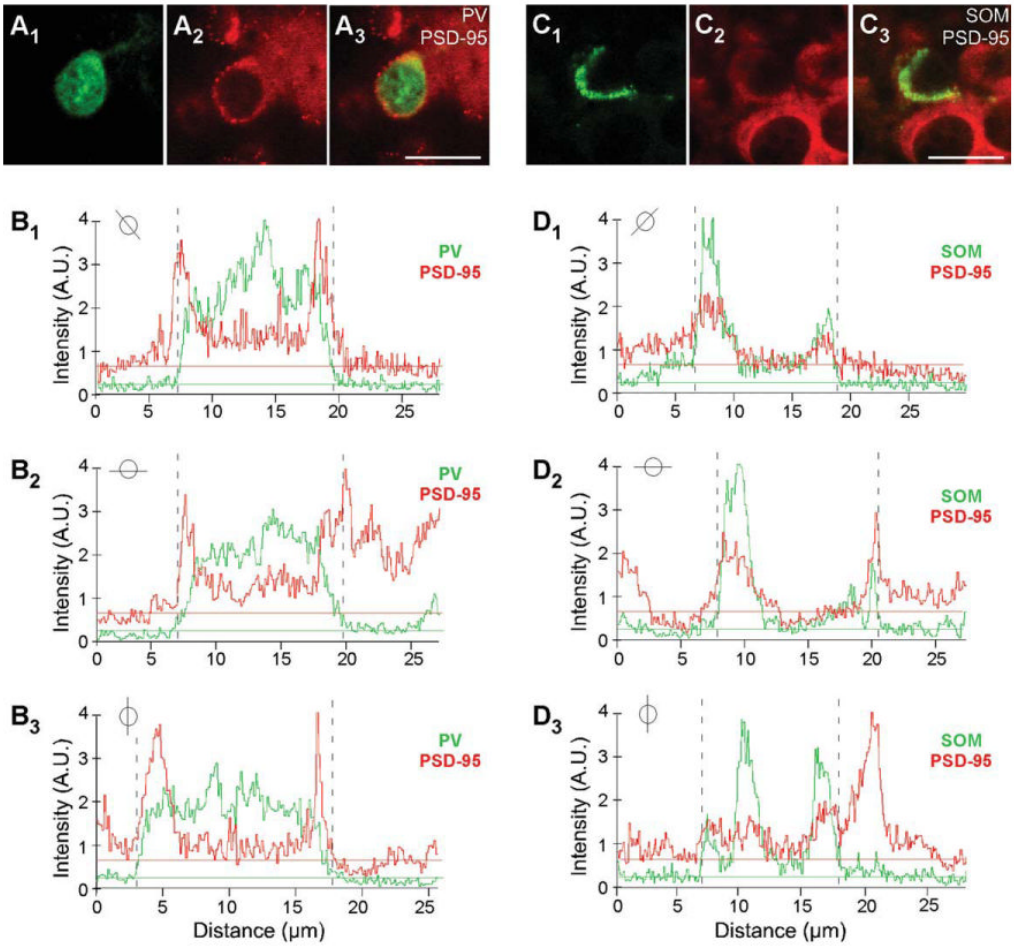

Figure 3.

Colocalization analysis of PSD-95 and PV or SOM. **A1-A3:** Confocal images of a juvenile (P15) mouse brain section labeled with rabbit anti-PV (green) and hybridized with DIG-labeled PSD-95 riboprobe (red; enlarged version of Fig. 1B1–B3). Note the halo/ring around the apparent nucleus. B1–B3: Plots of the signal intensities of PV (green) and PSD-95 (red) for a line that cuts through the immunopositive (PV^+) cell for the images in (A1–A3; the specific line through the cell is indicated in the small circle inset). The horizontal lines show the average baseline signal intensity for PV (green) and PSD-95 (red; see Materials and Methods). The region where PV signal is greater than the baseline (dashed lines on graphs) is identified as a PV^+ interneuron. Note that the peak PSD-95 signal matches and overlaps with the PV signal, except for the nucleus, where PV is present but PSD-95 is not. **C1–C3:** Confocal images of a juvenile (P15) mouse brain section labeled with rat anti-SOM (green) and hybridized with DIG-labeled PSD-95 riboprobe (red; enlarged version of Fig. 1E1–E3). **D1–D3:** Plots of the signal intensities of SOM (green) and PSD-95 (red) for a line that cuts through the immunopositive (SOM^+) cell for the image in (C1–C3; see small circle inset). Note that the SOM signal is not uniformly present around the soma. A.U., arbitrary units. For magenta-green images see Supporting Information Figure 9. Scale bars = 20 μm

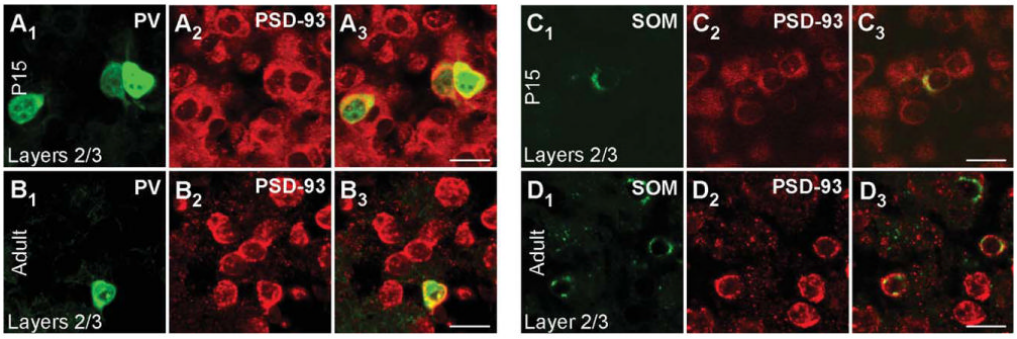

Figure 4.

PSD-93 mRNA expression in PV^+ and SOM^+ interneurons in the mouse visual cortex. Confocal images of combined in situ hybridization and immunohistochemistry for PSD-93 and PV or SOM in the mouse visual cortex. Tissue sections were obtained from juvenile (P15; **A1–A3,C1–C3**) or adult (**B1–B3,D1–D3**) mouse visual cortex. In the left columns, sections were labeled with either rabbit anti-PV (A1,B1) or rat anti-SOM (C1,D1; green). In the middle columns (A2,B2,C2,D2), the same sections were hybridized with DIG-labeled PSD-93 riboprobe (red). The right columns (A3,B3,C3,D3) show merged images. Images are at ×63. For magenta-green images see Supporting Information Figure 10. Scale bars = 20 μm.

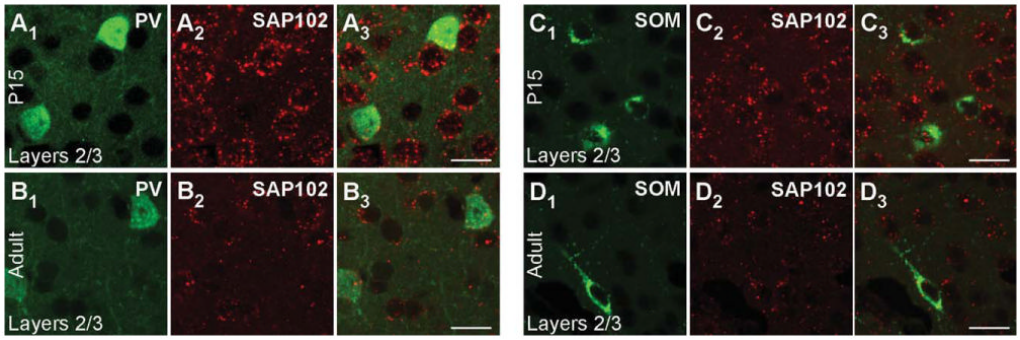

Figure 5.

SAP102 mRNA expression in PV^+ and SOM^+ interneurons in the mouse visual cortex. Confocal images of combined in situ hybridization and immunohistochemistry for SAP102 and PV or SOM in the mouse visual cortex. Tissue sections were obtained from juvenile (P15; **A1–A3,C1–C3**) or adult (**B1–B3,D1–D3**) mouse visual cortex. In the left columns, sections were labeled with either rabbit anti-PV (A1,B1) or rat anti-SOM (C1,D1; green). In the middle columns (A2,B2,C2,D2), the same sections were hybridized with DIG-labeled SAP102 riboprobe (red). The right columns (A3,B3,C3,D3) show merged images. Images are at ×63. For magenta-green images see Supporting Information Figure 11. Scale bars = 20 μm.

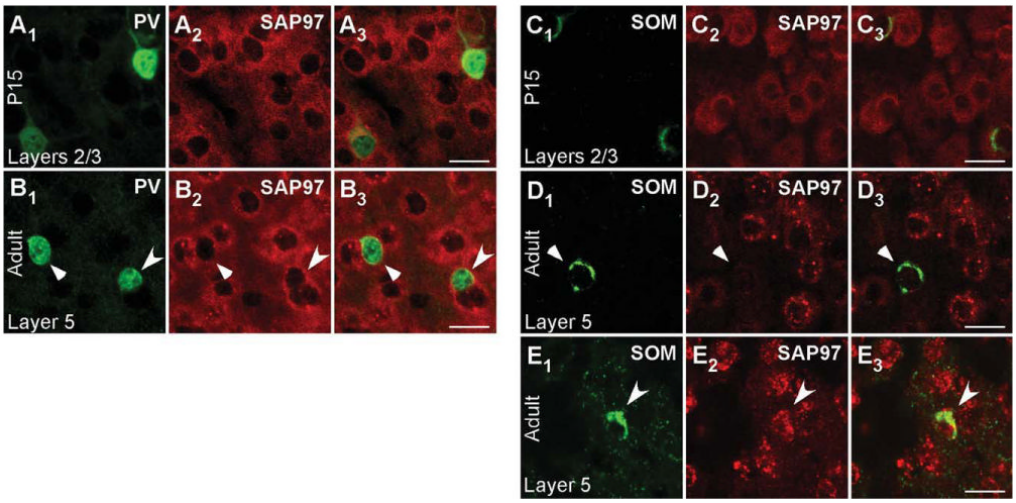

Figure 6.

Developmentally regulated expression of SAP97 mRNA in PV^+ and SOM^+ interneurons in layers 2/3 of the mouse visual cortex. Confocal images of combined in situ hybridization and immunohistochemistry for SAP97 and PV or SOM in the mouse visual cortex. Tissue sections were obtained from juvenile (P15; A1–A3,C1–C3) or adult (B1–B3,D1–E3) mouse visual cortex. In the left columns, sections were labeled with either rabbit anti-PV (A1,B1) or rat anti-SOM (C1,D1,E1; green). In the middle columns (A2,B2,C2,D2,E2), the same sections were hybridized with DIG-labeled SAP97 riboprobe (red). Our riboprobe detected both spliced isoforms (α and β) of SAP97. The right columns (A3,B3,C3,D3,E3) show merged images. Images are at ×63. For adult tissue images (B1–B3,D1–E3), triangles point to PV^+ and SOM^+ interneurons that are negative, and arrowheads point to interneurons that are positive for SAP97 mRNA. For magenta-green images see Supporting Information Figure 12. Scale bars = 20 μm.

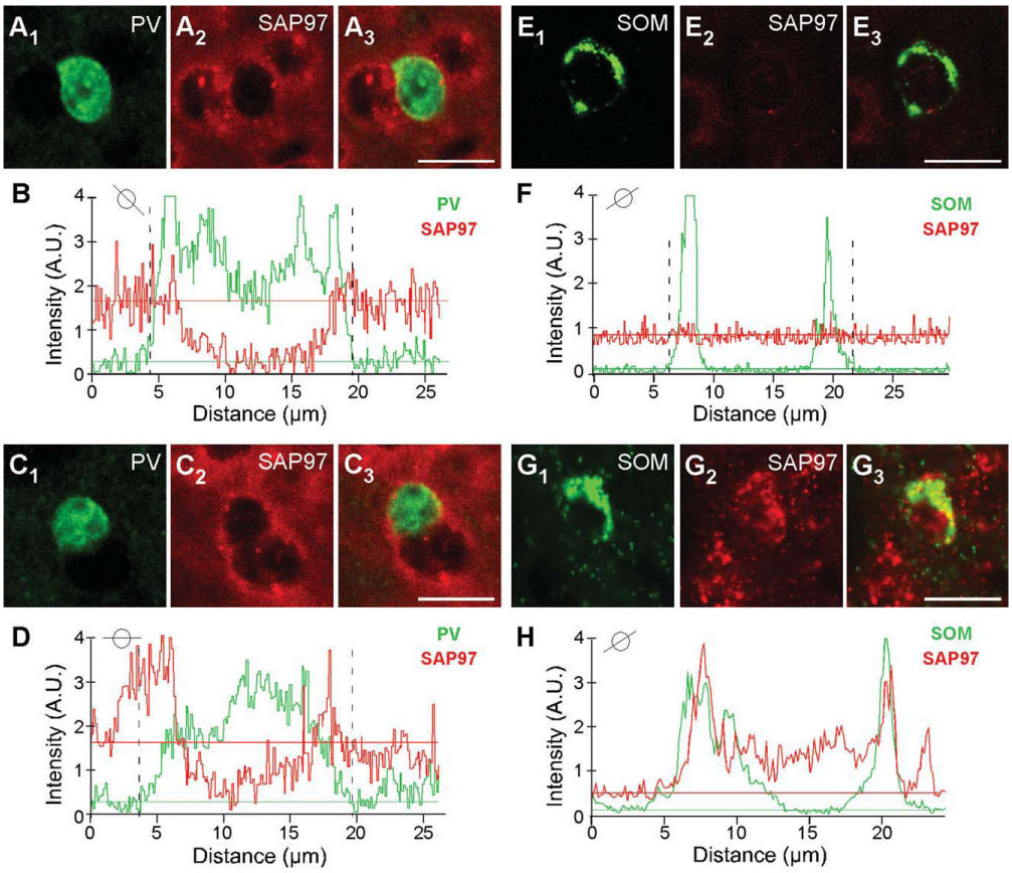

Figure 7.

Colocalization analysis of SAP97 and PV or SOM. A1–A3,C1–C3: Confocal images of an adult mouse brain section labeled with rabbit anti-PV (green) and hybridized with DIG-labeled SAP97 riboprobe (red; enlarged version of Fig. 6B1–B3). B,D: Plots of the signal intensities of PV (green) and SAP97 (red; B, low expressing; D, high expressing) for a line that cuts through each of the immunopositive (PV^+) cells (see small circle insets). The analysis is identical to that in Figure 3. In B, a peak SAP97 signal relative to its baseline is difficult to identify, and the PV^+ cell was scored negative. Note that, in this instance, we avoided drawing analysis lines that went through the adjacent non-PV^+ cells. In D, although there are background complications, a peak SAP97 signal could be associated with the PV signal. **E1-E3,G1-G3:** Confocal images of an adult mouse brain section labeled with rat anti-SOM (green) and hybridized with DIG-labeled SAP97 riboprobe (red; enlarged version of Fig. 6D1-D3,E1-E3). **F,H:** Plots of the signal intensities of SOM (green) and SAP97 (red; F, low expressing; H, high expressing) for a line that cuts through each of the immunopositive cells (see small circle insets). A peak SAP97 signal was not present, and the SOM^+ cell was scored negative. In H, the peak SAP97 signal matches and overlaps with the SOM signal. A.U., arbitrary units. For magenta-green images see Supporting Information Figure 13. Scale bars = 20 μm.

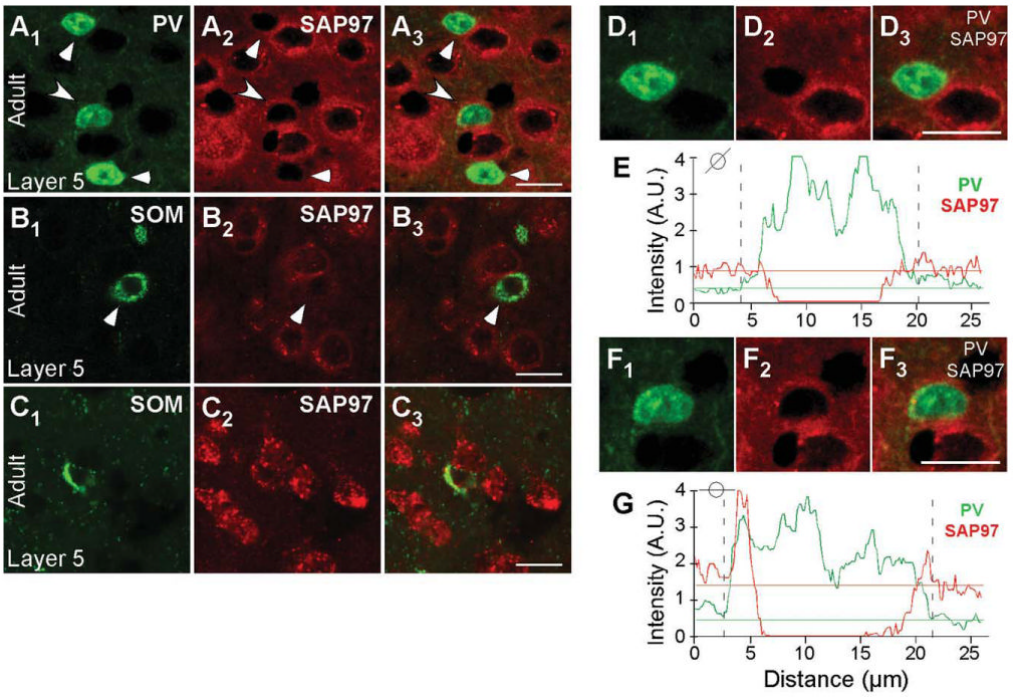

Figure 8.

Developmentally regulated expression of SAP97 mRNA in PV^+ and SOM^+ interneurons in layers 5 of the mouse visual cortex. Confocal images of combined in situ hybridization and immunohistochemistry for SAP97 and PV or SOM in the mouse visual cortex. Tissue sections were obtained from adult mouse visual cortex. In the left column, sections were labeled with either rabbit anti-PV (A1) or rat anti-SOM (B1,C1; green). In the middle column (A2,B2,C2), the same sections were hybridized with DIG-labeled SAP97 riboprobe (red). The right column (A3,B3,C3) shows merged images. Images are at ×63. Triangles point to PV^+ and SOM^+ interneurons that are negative, and arrowheads point to interneurons that are positive for SAP97 mRNA. D1-G: Enlarged versions of the two cells (D1-D3,F1-F3) in A1-A3 and the plots of the signal intensities of PV (green) and SAP97 (red; E, low expressing; G, high expressing) for a line that cuts through each of the immunopositive (PV^+) cells (see small circle insets). In G, the peak SAP97 signal is associated with the PV signal. A.U., arbitrary units. For magenta-green images see Supporting Information Figure 14. Scale bars = 20 μm.

Table 1
Primary Antibodies Used in the Present Study

Antigen	Immunogen	Antibody information	Dilution used
Parvalbumin (rabbit anti-PV)	Purified rat skeletal muscle parvalbumin	Abcam (Cambridge, MA), rabbit polyclonal, ab11427	1:1,000
Somatostatin (rat anti-SOM)	Synthetic 1-14 cyclic somatostatin conjugated to bovine thyroglobulin using carbodiimide	Chemicon (Temecula, CA), rat monoclonal, MAB354	1:200

Table 2

Colocalization of MAGUKs in PV$^+$ and SOM$^+$ Interneurons in the Mouse Visual Cortex[1]

		P15		Adult	
		No.	%	No.	%
Layers 2/3	PSD-95	32 (32)	100	66 (66)	100
	PSD-93	59 (62)	95	104 (110)	95
PV$^+$	SAP97	53 (54)	98	38 (97)	39
	SAP102	91 (93)	98	147 (161)	91
Layer 5	PSD-95	28 (29)	97	90 (95)	95
	PSD-93	69 (71)	97	109 (121)	90
PV$^+$	SAP97	46 (54)	85	29 (74)	39
	SAP102	85 (88)	97	117 (135)	87
Layers 2/3	PSD-95	74 (74)	100	83 (88)	94
	PSD-93	101 (108)	94	45 (51)	88
SOM$^+$	SAP97	48 (51)	94	35 (107)	33
	SAP102	91 (93)	98	147 (161)	91
Layer 5	PSD-95	114 (117)	97	38 (38)	100
	PSD-93	87 (90)	97	34 (42)	81
SOM$^+$	SAP97	24 (25)	96	22 (65)	34
	SAP102	86 (87)	99	63 (64)	98

[1] No. refers to the numbers of cells that were PV$^+$ or SOM$^+$ and positive for the particular MAGUK. Total number of cells screened for each condition is indicated in parentheses. At minimum, three different animals were measured for each condition.

J Comp Neurol. Author manuscript; available in PMC 2011 December 12.